FliPASED
WWW.FLIPASED.EU

D1.1 Wing and demonstrator actuation and sensing conceptual design requirements
D. Teubl (TUM)

GA number:	815058
Project acronym:	FLIPASED
Project title:	FLIGHT PHASE ADAPTIVE AEROSERVO-ELASTIC AIRCRAFT DESIGN METHODS
Funding Scheme: H2020	**ID:** MG-3-1-2018
Latest version of Annex I:	1.1 released on 12/04/2019
Start date of project: 01/09/2019	**Duration:** 40 Months

Lead Beneficiary for this deliverable:	TUM
Last modified: 02/12/2020	**Status:** Delivered
Due date: 31/10/2020	

Project co-ordinator name and organisation:	Bálint Vanek, SZTAKI
Tel. and email: **+36 1 279 6113**	vanek@sztaki.hu
Project website:	www.flipased.eu

Dissemination Level		
PU	Public	X
CO	Confidential, only for members of the consortium (including the Commission Services)	

“This document is part of a project that has received funding from the European Union’s Horizon 2020 research and innovation programme under grant agreement No 815058.”

Glossary

AC Aircraft. 44

ACMU Actuator Control and Monitoring Unit developed at TUM. 31, 32, 33

ADC Analog Digital Converter. 16, 19, 21

CAN Control Area Network. 7, 13

ESD Electrostatic Discharge. 15

FCC Flight Control Computer. 15, 17, 31, 32, 34, 39

FLEXOP Flutter Free Flight Envelope Expansion For Economical Performance Improvement. 8, 13, 17, 18, 19

FlightHAT Part of the FCC developed by SZTAKI. 16

GNSS Global Navigation Stallite System. 4, 21, 23

GPIO General Purpose Input Output. 16

GPS Global Positioning System. 21, 23

GUI Graphical User Interface. 15

GVT Ground Vibration Test. 13

ICSP In Circuit Serial Programming. 14

IMU Intertial Measurement Unit. 13

ISM-band Industrial, scientific and medical purposes radio bands. 21, 23

MEMS Micro-Electo-Mechanical systems. 29, 30

PCB Printed Circuit Board. 30

PPM Pulse Position Modulation. 14

PSU Power Supply Unit. 15

PWM Pulse Width Modulation. 13, 14, 15

RC Remote controlled. 13, 14, 15

RX-MUX I/O control signal switch unit devloped by SZTAKI. 7, 13

SBC Single Board Computer. 17

SHM Servo Health Monitor. 14

SPI Serial Peripheral Interface. 16

SSI Stochastic Subspace Identification. 17

UAV Unmanned Aerial Vehicle. 24

Table of contents

List of Figures

1 Executive Summary

This document collects together the proposed conceptual designs for sensor layout and actuation system of the wing (3), and the improvements made and proposed on the fuselage based on operational experience.

During integration and operation of the aircraft the operation team found a couple of design related problems which either made the operation unsafe like the landing gear, or give too harsh boundary for critical function implementation like the lack of digital remote control interface on the RX-MUX units. Along with that, some additional changes are already made to improve the existing functionality like secondary on board computer, and further changes are proposed to have even increased functionality like electrical power measurement or High bandwidth telemetry system. The second chapter introduce these changes more in depth.

The third section is dedicated to the wing (3) sensor layout and actuation system. Along with the inertial measurement units used on previous wings other sensor layout concepts are proposed. On flight control and actuator system side, a CAN bus based actuator system is proposed. Along with that a detailed comparison is given between the proposed design and the system used on previous wings during the legacy FLEXOP project.

The forth chapter is dedicated to the experiences and detailed study on the servo health monitoring system currently used in the -0, -1 and -2 wings.

The main contributions of this documents are:

- It collects the main changes proposed in the fusealge, compared to original design documents
- Provides an updated sensor layout concepts for wing (3).
- Provides actuator system concept for wing (3).
- Shows a detailed analysis of the previously used servo health monitoring tools system.

2 Fuselage

2.1 Landing gear

Building on previous experience, landing gear proved to be one of the biggest challenges during the operation of the demonstrator. The aircraft proved to be difficult to control while on the ground, leading to a few very dangerous situations and one accident, where the aircraft skidded of the runway and hit a runway light.

While trying to solve the ground handling problem, the following design mistakes were identified:

- The maximum angle of attack, achieved on the ground, is limited by very low main landing gear and a reasonably tall tail wheel. This design solution limits the maximum angle of attack, that could be achieved for takeoff, to 3.3deg. This is unusually small for a taildragger aircraft and usually would be around 10deg. In addition, such solution is also very hard to change on an already manufactured aircraft.
- Very narrow main landing gear makes it easy for the aircraft to bank from wingtip to wingtip. If this happens during takeoff or landing, the wingtip touches the ground and instantly creates a destabilizing moment.
- Main landing gear is quite far from the center of gravity. This means that the disturbing bank angle, required to tip the aircraft, is further decreased.
- The tires of the main landing gear are too soft for the airplane. This makes it possible to deform the tires very easily and also significantly increases the rolling resistance during take-off run.
- Unsteerable tail wheel makes the aircraft very hard to control while on the ground. The tail has to be lifted up first and aircraft is then steered with the rudder.
- Retractable main landing gear proved to be an unnecessary design add-on to the aircraft which adds complexity, but not value to the demonstrator overall.

These problems were hard to identify during the conceptual or preliminary design phase of the FLEXOP project and were only realized during operations. Therefore further discussion was held how to make the controllability of the aircraft better.

Two different concepts were discussed:

- Fundamentally changing the landing gear layout.

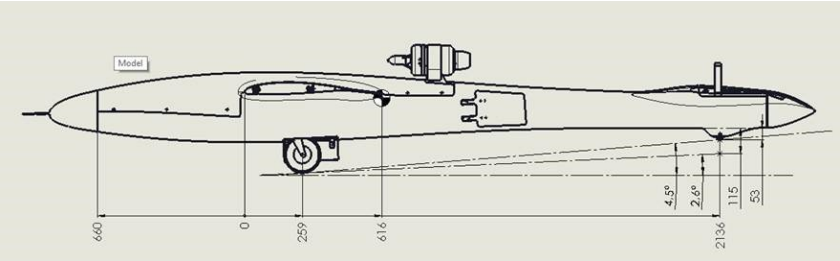

Figure 1: Sketch of the attainable angle of attack during the take-off run. 4.5deg is the maximum fuselage incidence angle. The wing incidence is -1.2deg. The 2.6deg is the resulting maximum angle of attack after the steerable tailwheel modification is done.

- Adjusting the current landing gear to make it acceptably safe for operation.

But because of the fact that the first option would require major fuselage changes and would take at least a few months, it was decided to start with the second option first.

Ways to improve handling were discussed during the winter before the first flight test campaign. Due to the complex nature of the problem the solutions that were initially agreed upon did not completely resolve the issue. This resulted in an iterative process with different concepts being implemented as add-ons to the initial design along the way. The chronology of the process was:

- Implement the steerable tailwheel with damping
  - The initial solution to steering was to install an off-the-shelf tailwheel assembly. Unfortunately the solution did not work because the load on the tailwheel appeared to be too big for the part. Therefore another, completely custom iteration was done. This included a custom milled aluminum fork for steering and also a damping assembly. The damping assembly was composed of glass-fiber-reinforced plastic plate acting as a leaf spring for longitudinal damping and two rubber dampers for lateral stiffness 2. The structure held well, but the steering made the aircraft hard to control and very sensitive to any pilot inputs.
- Change the brakes of the main landing gear to more effective ones
  - Tire brakes were changed into drum brakes. From previous testing it was noted that the tires wear out very quickly due to the brakes. Also the braking power of the old system proved to be too little. Therefore new type of brakes were implemented that would both conserve the tires and increase the braking force on the wheel hub.
- Add a gyro to the tailwheel

  - Introducing the steerable tailwheel did not solve the controllability problem as the team has hopped. The aircraft became very sensitive, especially at higher speeds. The solution was to introduce a gyroscope-based compensation for the gain on the steering. This proved to improve the steering somewhat.

- Reverse the main landing gear frame to shift the ground contact point back

  - One of the main findings, mentioned in the early research on taildragger aircraft is that the tendency to veer of the runway is decreased if the centre of gravity is kept as close as possible to the main landing gear. This was recorded in all of the reports on the topic. Therefore changing the location of the landing gear was considered. Luckily, the landing gear frame was easy to flip, moving the main landing gear backwards by 75mm 3. The outcome was lesser tendency to veer off the runway, an increase to the critical bank angle to tip on one wing, but also higher load on the main tires. Even though the weight increase was only 2.5 per cent per wheel, the main tires were already overloaded. Therefore further steps would include looking for stiffer main tires, if possible.

- Laterally stiffen the main landing gear assembly

  - During the taxi tests cameras were mounted facing both the gears 4 5. This helped to observe the behavior of the landing gear and make further conclusions. One of them was that the main landing gear is too flexible laterally, which makes it easier to tip onto one wing and also harder to get out of the tipped position. Therefore further stiffening parts were introduced to stiffen the landing gear laterally.

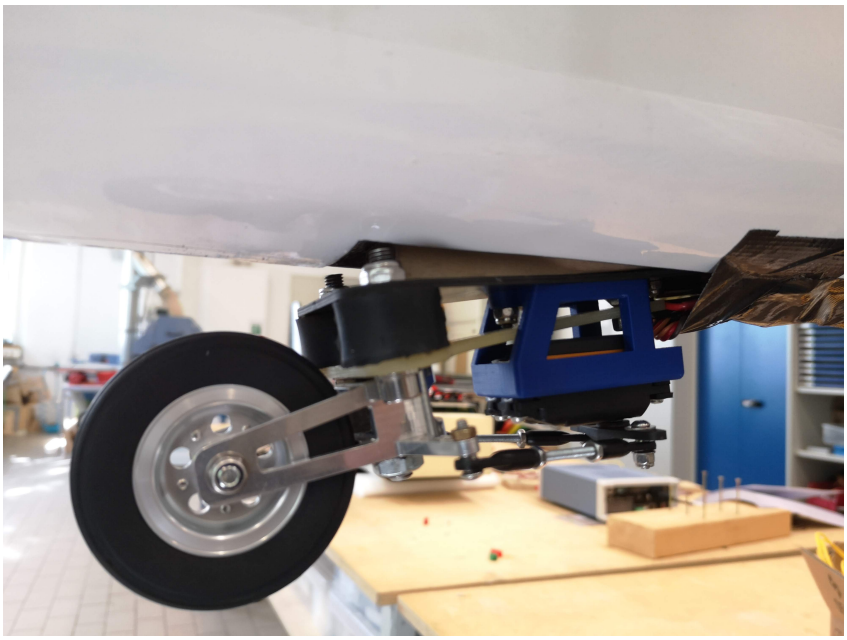

Figure 2: The implemented steerable tailwheel.

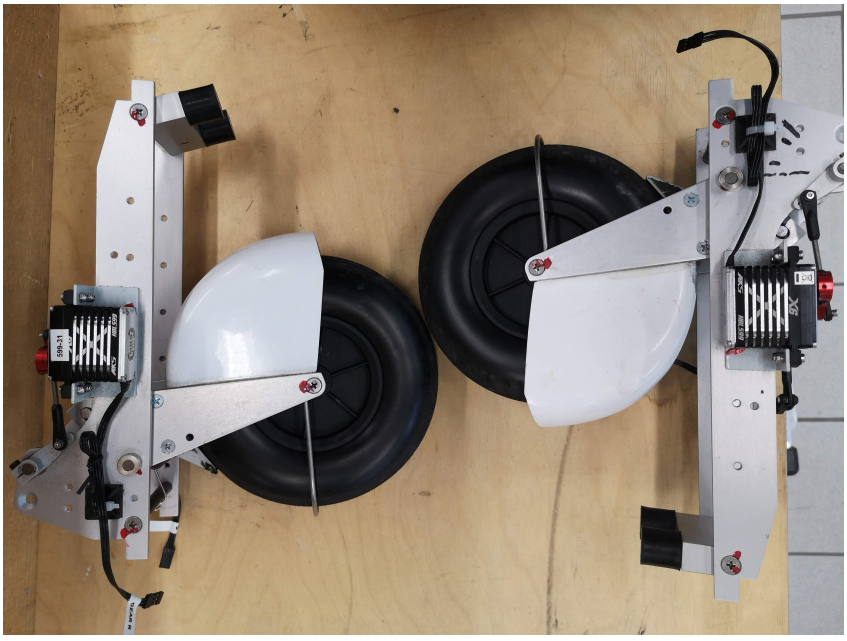

Figure 3: The comparison of main wheel position when normal and flipped. The difference is 75mm.

Figure 4: The camera facing main landing gear during taxi testing.

Figure 5: The camera facing tail wheel during taxi testing.

2.2 Sensor configurations

Based on results from the Ground Vibration Test (GVT) it was decided to instrument the empenage and fuselage with additional IMUs, as shown in Figure 6. One IMU in each tail measuring acceleration in three directions will enable the identification of 4 v-tail modes in the bandwidth 17 Hz - 33 Hz. The IMUs should be located as far from the root as possible. The sensors are oriented in the global reference frame in Figure 6, however a local coordinate system is easier to manufacture and together with Euler angles serves the same purpose. For the purpose of modal analysis no angular rates are required on the IMUs in the empenage or fuselage, thus saving bandwidth on the CAN bus.

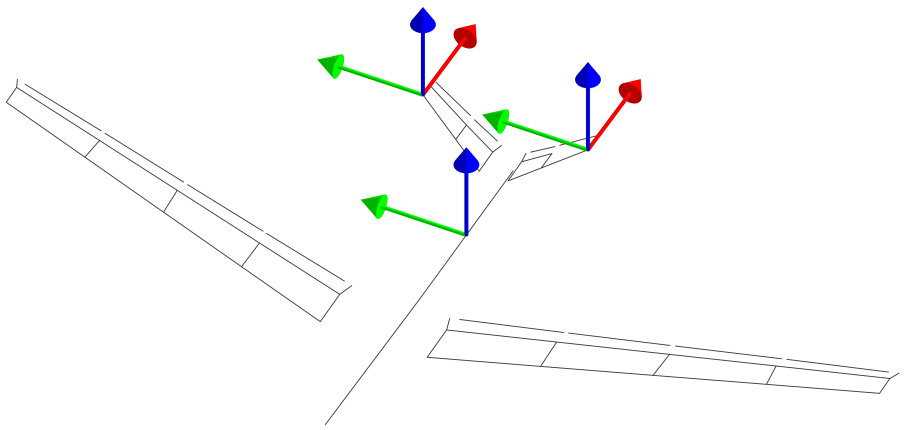

Figure 6: IMU empenage configuration.

2.3 RX-MUX unit

The primary task of the RX-MUX is to provide reference signals for the actuators and to switch between signal sources. There are three different signal sources: the RC transmitters of the two pilots and the Raspberry Pi, which runs the autopilot software. It can be manually set whether it uses the transmitters or the Raspberry Pi as a signal source. If the primary RC transmitter loses the connection with the aircraft, the secondary will take its place. Moreover, even if one of the RX-MUXs breaks down the aircraft will remain controllable. Each of the RX-MUXs has its own power supply and they work independently.

During the FLEXOP project RX-MUXs used analog PWM signals to control the actuators which are more noise sensitive than digital protocols and one channel is capable of handling only one actuator. Along witht hat, feedback form the actuators are not

possible via PWM, so the SHM units had to be introduced for monitoring. Therefore, using digital communication protocol would increase the reliability of data transmission and one interface could communicate with multiply actuators.

The communication between the RX-MUX units and the RC transmitters are done via PPM (Pulse Position Modulation). A simple analog channel, which contaions PWM duty cycle informations up to 16 channels. Due to this upper limit of the PPM signal, the control functions via RC transmitter are very limited. Using digital communication can increase the number of individial channels up to 24, which would result in more functionalities for the pilots.

The older version of RX-MUX has limited number of digital interfaces, including CAN and UART. Moreover, based on the earlier experiences we had to rethink the RX-MUX-es programming, debugging and maintaining methods. The earlier version supported only ICSP(In Circuit Serial Programming), which made the development and configuration cumbersome procedure. Each RX-MUX-es on the stack required a unique software with the appropriated set of variables and we have to program them one by one. The figure 7 shows the new version of RX-MUX hardware.

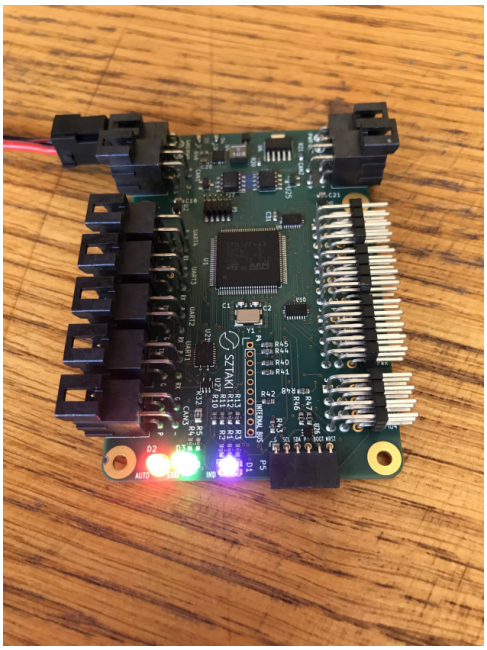

Figure 7: RX-MUX v2

2.3.1 Hardware

The RX-MUX version 1.0 based on a 16 bit PIC microcontroller, which has many limitation including the limited number of interfaces, computational power and complexity of the further feature implementation. It was necessary to rethink the power management, the connector types and the required interfaces as well. Using STM32F4 instead of the original PIC microcontroller provides a more robust and scalable so-

lution. Furthermore it decreases the complexity of development, thanks to the ST's code generation tools, detailed documentations and 32 bit architecture. The flightHAT also uses STM32F4 microcontroller, so the development toolchain of the FCC is also simpler. The new RX-MUX is compatible with its earlier version but it has more computation power and capable of handling more digital interfaces like digital radio control and digital actuators. The board has built in ESD (Electrostatic Discharge), over voltage, polarity protection and properly operate on battery and PSU (Power Supply Unit) as well. The boards different connectors are more durable and capable of managing more plug and unplug cycles.

2.3.2 Client application

We develop a client application, which will be able to connect to the RX-MUXs and updates their embedded software and configurations. The RX-MUXs can send status information to the client application in online state and the configuration of the actuators can be set. As we imagined the client software implementation contains two level of interfaces a developer and a user one. The developer interface is a batch of scripts, which provides the essential functions. The user interface is built on the scripts and implements a cross-platform GUI. The firmware update function uses the STM32F4 series built in I2C boot loader. As Figure!8 shows the client application is connected to the internal I2C bus where each of the RX-MUXs I2C address can be selected with a soldered jumper. Therefore, the RX-MUXs use the same software and during the initialization process they configure themselves for specific role.

2.3.3 Interfaces

The new RX-MUXs have extended number of CAN and UART interfaces, which will be able to control the actuators and receive digital signal from the RC receivers. There are more channels and interfaces than it is required, because if a new function is added in the future, RX-MUX 2.0 will have to be able to support it. The following list contains the required interfaces and their applications.

- *3 CAN(Controller Area Network):* Two CAN interfaces is reserved for the digital actuators and the third one for Direct Drive.
- *4 UART (Universal Asynchronous Receiver-Transmitter):* RC receivers analog signals will also be replaced with UART compatible receivers. Two UART interfaces can handling S-BUS[3] and Ex-BUS[5] protocols which are widely used by RC transmitters.
- *12 PWM (Pulse-Width Modulation) channels:* Analog actuators are controlled by PWM signals. An aircraft will be controlled by 2 or more RX-MUX-es due to safety critical considerations. Therefore we will have altogether 24 available PWM channels, which will be more than enough for FLiPASED aircraft and RX-MUX remain compatible with the earlier version.

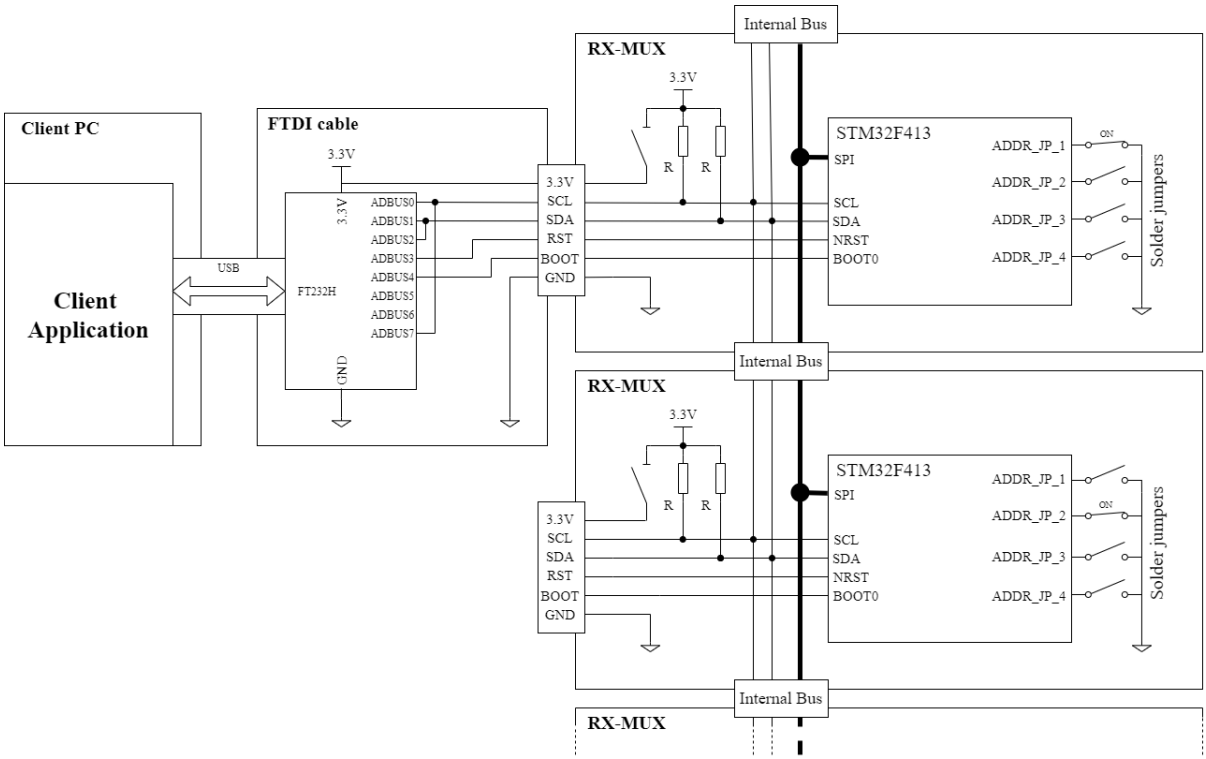

Figure 8: Client application and RX-MUXs communication interface

- *4 GPIO (General-Purpose Input/Output):* Including configurable Input Capture for the currently used Radio Control receivers and ADC (Analog Digital Converter) for the battery voltage measurement purposes. Future development might need some basic control what GPIO can provide.
- *1 Power LED (Light-Emitting Diode)*
- *1 Status LED:* Indicates whether the plane is in autopilot or manual mode.
- *1 RGB (Red Green Blue) LED:* Indicates events and errors.
- *SPI (Serial Peripheral Interface):* Communication with FlightHAT and clock synchronisation.
- *I2C (Inter-Integrated Circuit):* Communication between RX-MUXs and the client application

2.4 Secondary on-board computer

In order to perform real time modal analysis in flight an additional Single Board Computer (SBC) was integrated into the FLEXOP flight stack. A raspberry pi 4 was used due to its computational power to weight ratio as well as its ability to integrate seamless with the Flight Control Computer (FCC). The so called 'Flutterometer' receives data in real time from the FCC, builds a First In First Out (FIFO) buffer, performs modal analysis using the Stochastic Subspace Identification (SSI) technique, tracks the modes, and sends the data via a 433 MHz RF telemetry link to the ground station. The Flutterometer system is programmed in Python and runs on boot of the Linux OS from Crontab. No user interaction is therefore required. The Flutterometer receives power from the aircraft Lipo batteries and does not require additional connections or switching. The wifi is permanently disabled, and the code is maintained through git.

A housing for the Flutterometer was designed an 3D printed, as seen in Figure 9, to fit on top of the RX-MUX boards in the FLEXOP flight stack. The Flutterometer has a USB-C power connection and receives data via an Ethernet cable from the FCC. The Flutterometer (Raspberry pi 4) in the housing can be seen in Figure 10. Furthermore integration of the thrust measurement system and 5G telemetry link will be handled by the Flutterometer.

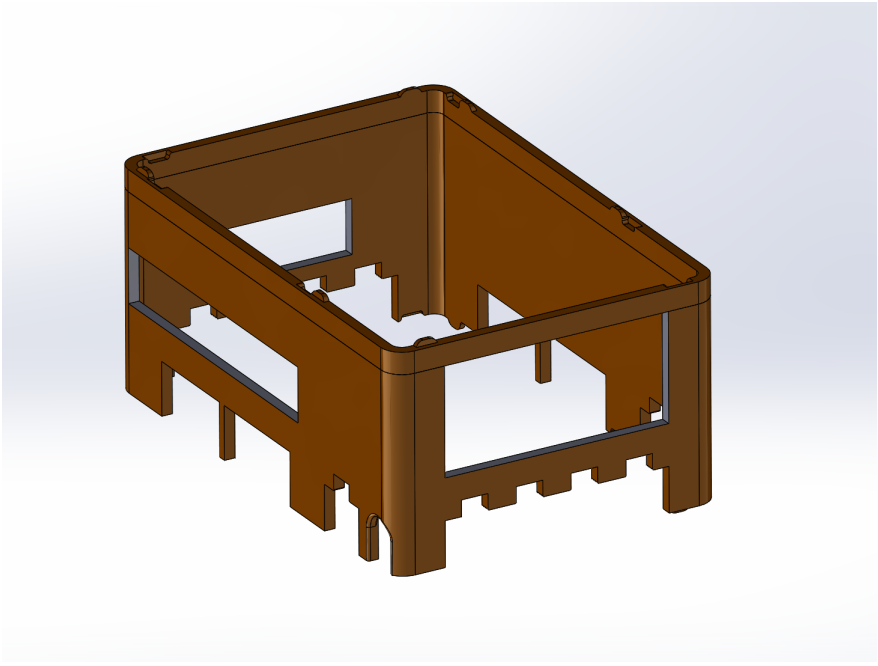

Figure 9: Flutterometer housing.

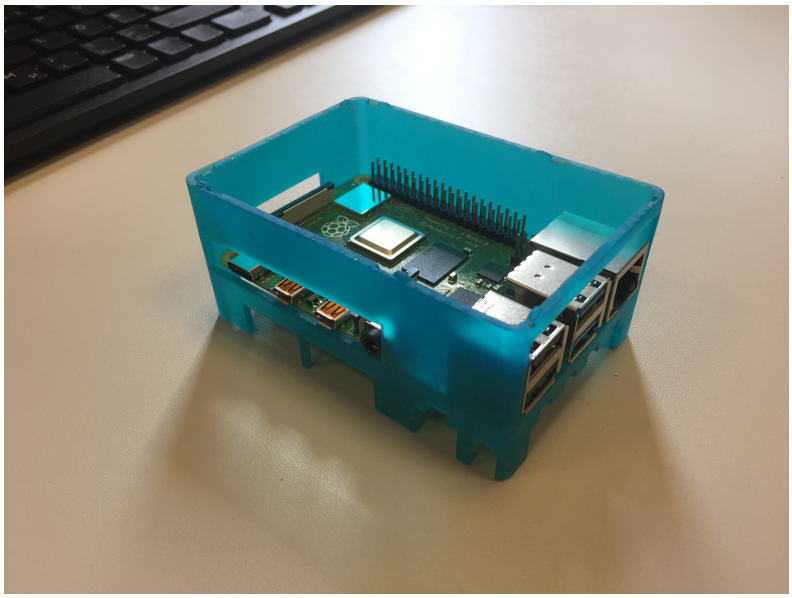

Figure 10: Raspberry pi 4 and housing.

2.5 Thrust measurement

To better evaluate the effects inflicted of alterations on the aircraft's drag, it is necessary to determine that aerodynamic force. This poses a challenge to the project because drag on aircraft is not directly mensurable. Instead, the force must be derived from the aircraft's equations of motion with the use of the flight parameters such as attitude, velocity and thrust.

Conversely, the in-flight thrust measurement not straightforward and must also be performed indirectly. Several methods have been developed and tested, whereas the most reliable require multiple sensors throughout the engine. These provide values that can be used to calculate the corresponding thrust. Such are known as gas-generator methods and are suitable for large aircraft, which have been designed with extensive sensory within the engine.

In contrast, smaller propulsion units such as the B300F that powers the FLEXOP demonstrator aircraft do not have provisions for the installation of pressure and temperature probes. Thus, the required modifications to the engine's structure hinder the viability of gas-generator methods. As an alternative, simplified and swinging probe methods were considered. These require no sensors inside the engine but are limited to gross thrust measurement, not sufficient for drag determination. Further, brochure and acoustic-based methods were studied but, due to limited data provided by the engine's manufacturer, calibration would be complex and limited reliability would be achievable.

Consequently, the trunnion thrust method was the option chosen as the most viable for a thrust measurement system to be installed on the FLEXOP aircraft. This technique is usually not considered feasible for larger aircraft due to the high complexity of the engine attachments, including multiple connection points as well as cables, pipes and hoses that make load path determination difficult. However, for a small aircraft, the attachment structure can be significantly simplified without affecting other systems and having higher design flexibility. As a result, the trunnion thrust method is suitable for this type of aircraft.

Accordingly, a new attachment structure between the B300F engine and the aircraft's body was designed, whereas particular attention was given to obtaining a well-defined path for load transmission. More specifically, the structure was designed to form a statically determinate system when modeled in the aircraft's XZ-plane (symmetry plane). Thus, it is possible to determine the thrust force by measuring the load at a single support point with a load cell.

Moreover, alternatives that kept the measuring system simple were preferred. For this reason, interference from varying vertical and lateral force components during flight maneuvers is not counteracted by implementing multi-axial load cells or devices that offer compensation for off-center and lateral loading. Instead, the support to which the load cell is installed was designed to only transmit forces in the measurement direction. This was achieved by implementing the support as two heim joints with the s-beam load cell installed between them. Thus, sensory complexity was kept low and bulky and heavy electronic components were avoided.

Additionally, the mentioned support was placed in the aircraft's symmetry plane to limit effects caused by thermal expansion, which have been a factor in previous attempts to implement the trunnion thrust method. In comparison, the other support points were implemented as rolling- element bearings placed on the sides of the structure. This allowed increased lateral stiffness for safer handling of the unit during maintenance operation but maintained the mechanical characteristics in the symmetry plane. Also, the configuration allows for low friction, which has been identified in previous projects as crucial for limiting the bending moments transmitted by the bearings and for allowing precise measurements. The final design is displayed by figure 11.

The structure was also designed with high measurement accuracy as a goal. For this reason, the positioning of the components was defined such that it minimizes errors. In fact, due to the ratio between the relative distances of the support points to the engine's center, all errors induced by the load cell and the analog-to digital (ADC) conversion are nearly halved. This was shown by an error estimation performed using data provided by the load cell's manufacturer to predict the deviation between the actual applied Thrust and the expected measured value, as shown by the diagram on figure 12.

According to the diagram, the system would deliver an accuracy of about 0.4N and

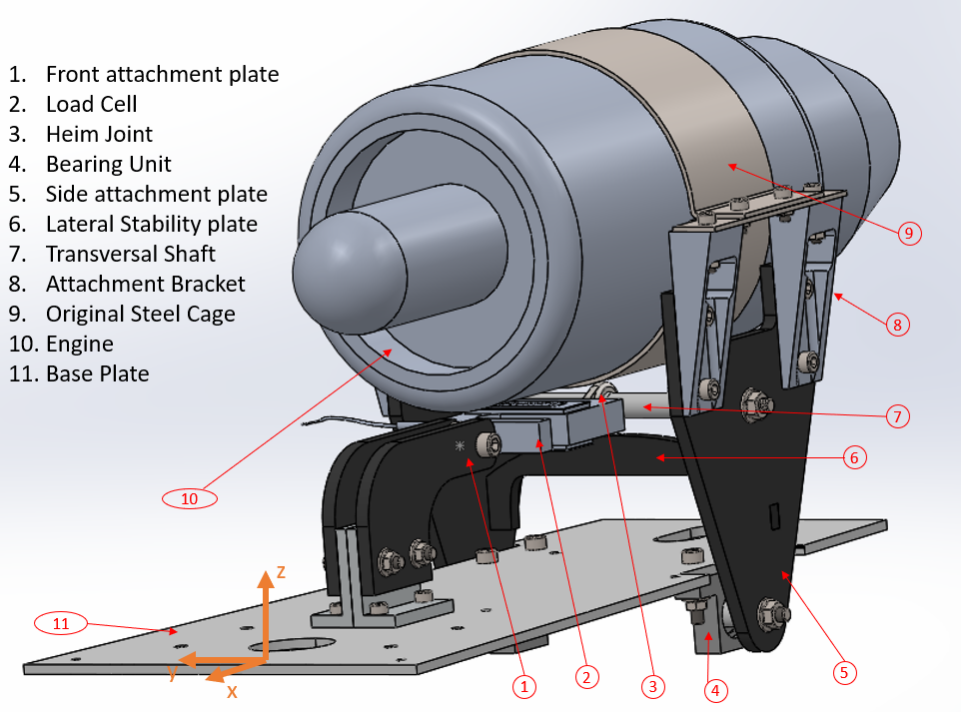

Figure 11: CAD model of engine attachment with thrust measurement system

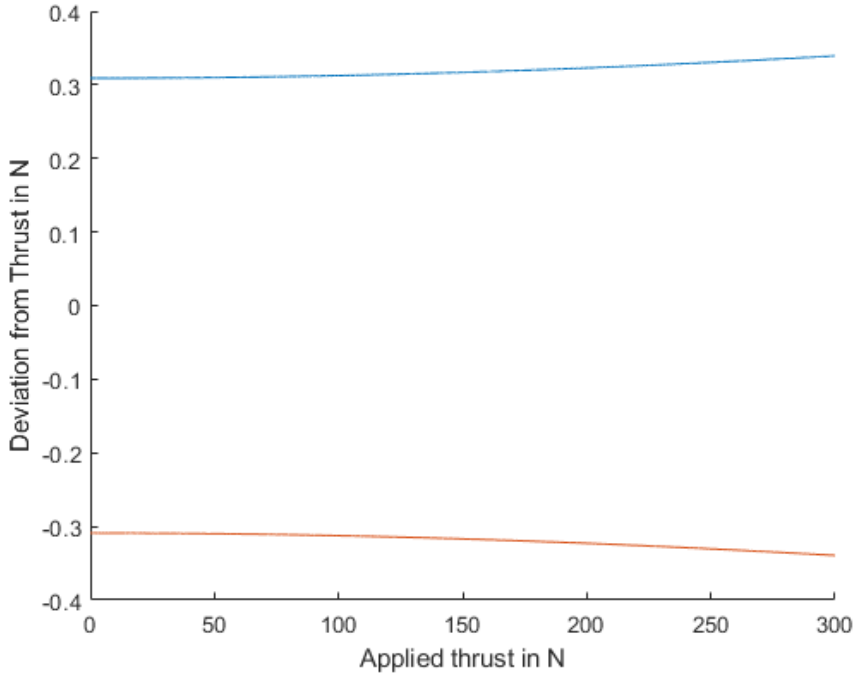

Figure 12: Expected upper (blue line) and lower (red line) deviation between applied and measured thrust

better at lower thrust levels. However, this estimate accounts only for load cell errors as well as ADC quantization and amplifier drift error. Therefore, additional influences such as higher temperature oscillations, manufacturing tolerances and further errors from the ADC (e.g. noise) may lead to lower performance and must be considered for a more accurate and extended prediction.

2.6 Electric power consumption measurement

Currently on energy point of view, only the fuel consumption is measured. Having power consumption measurement data for each mission is good feature, and can be used for future research. Although in the current state of the avionics system, it is a teadious process to acquire this data, and it is only possible to have overall power consumption.

To extend the measurement capabilities of the demonstrator, an independent power-consumption measurement devices is proposed, which will have the following main functions.

- Measure voltage and current of batteries — up to 4 batteries
- Log data into and SD card
- Provide telemetry stream to the secondary avionics
- Has access to GNSS time

2.7 High-bandwidth telemetry system

In order to implement more efficient flight testing routines by enabling online evaluation of acquired data and test adjustments during flight, a 5 GHz-Wifi Datalink has been developed and successfully field-tested up to ranges of 700 m without noticeable loss of data packages. For the tests, a different aircraft was used, which has a Rasprberry 4 on-board computer for data collection, thus has identical hardware interface to the secondary on-board computer.

The ISM-band-band of 5 GHz has been chosen for its high bandwidth as well as distance to ISM-band-bands already in use on the demonstrator.
The setup consists of a light and inexpensive Wifi-USB-dongle as the airborne unit and an antenna-tracker featuring a high-gain patch-antenna as the ground unit (Figure 13).

The alignment of the antenna towards the flying demonstrator is implemented based upon the GPS-positions of both the demonstrator and the antenna-tracker. Additionally

Figure 13: The antenna-tracker being prepared for field tests.

to the alignment of the antenna a camera can be used to document the flight tests or to give the crew of the Ground Control station better situational awareness in order to reduce interference and insure safe operation.

In order to utilize the data streaming from the demonstrator, NASA's OpenMCT visualization framework [1] is being implemented, with working examples already field-tested and deployed during flight tests. The OpenMCT framework allows the quick creation and adjustment of data displays that allow for the rapid adjustment of displays for the flight test at hand. Being in use in a variety of NASA's space programmes, the OpenMCT framework is under constant maintenance and development.

In a first step, a non-flight-critical, redundant data link will be implemented that will duplicate the data of the Engineering Data Link, as well as data relevant for system identification. Thus operational experience will be gathered, before more and more functionality will be implemented.

Additionally to the high-bandwidth downlink, the Ground Control Station is in the process of being equipped with a mobile Internet receiver, that will be able to establish connectivity to the internet. Thus, the foundation is laid to leverage the expertise persistent in the consortium in a broader way. Using the setup, data can be streamed live to partners in Europe, that can analyze the data as the flight test are conducted. Expected benefits are shorter feedback cycles on data quality and faster adjustments to changed or refined requirements.

In order to implement more efficient flight testing routines by enabling online evaluation of acquired data and test adjustments during flight, a 5 GHz-Wifi Datalink has been developed and successfully field-tested up to ranges of 700 m without noticeable loss of data packages. The ISM-band-band of 5 GHz has been chosen for its high bandwidth as well as distance to ISM-band-bands already in use on the demonstrator.

The setup consists of a light and inexpensive Wifi-USB-dongle as the airborne unit and an antenna-tracker featuring a high-gain patch-antenna as the ground unit (Figure 13).

The alignment of the antenna towards the flying demonstrator is implemented based upon the GPS-positions of both the demonstrator and the antenna-tracker. Additionally to the alignment of the antenna a camera can be used to document the flight tests or to give the crew of the Ground Control station better situational awareness.

2.8 ATK GNSS position dual antenna system

Figure 14 and figure 15 show the devices with details.

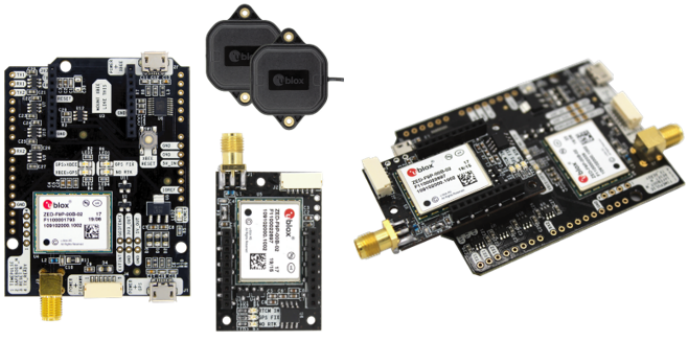

simpleRTK2B weight	20 g
simpleRTK2B dimensions	69 x 53 mm
simpleRTK2Blite weight	7.8 g
simpleRTK2Blite dimensions	41 x 28 mm
Navigation rate with RTK heading	8 Hz
Precision with NTRIP corrections	<1 cm
Precision with SSR corrections	<4 cm
RTK heading precision	0.4 deg with 1 meter distance between antennas

ZED-F9P Moving base applications

Figure 14: simpleRTK2B+heading - Basic Starter Kit

2.8.1 Hardware placement and integration

The two helix antennas are positioned in the centre line of the UAV (as figure 16 shows), the baseline length is 1 meter. The Ardusimple boards are placed in the fuselage and they are connected to the Flight Control Computer. The boards can communicate on USB, UART and they have Pixhawk connectors. The RTK positioning needs NTRIP corrections from a permanent ground station. The RTK heading is realized between the Ardusimple boards. The RTK positioning and heading information is useable for high accuracy and high frequency navigation updates. The integration of the RTK data and the inertial sensor measurements provides a reliable navigation system for the control of the UAV.

Product:	Outdoor Antennas
Application:	Beidou, Galileo, GLONASS, GPS
Mechanical Style:	Helical
Mounting Style:	Screw Mount
Length:	2.5 cm
Width:	2.5 cm
Height:	5.56 cm
IP Rating:	IP67
Antenna Connector Type:	SMA Male
Unit Weight:	50 g

Figure 15: Lightweight helical antenna for multiband GNSS (IP67)

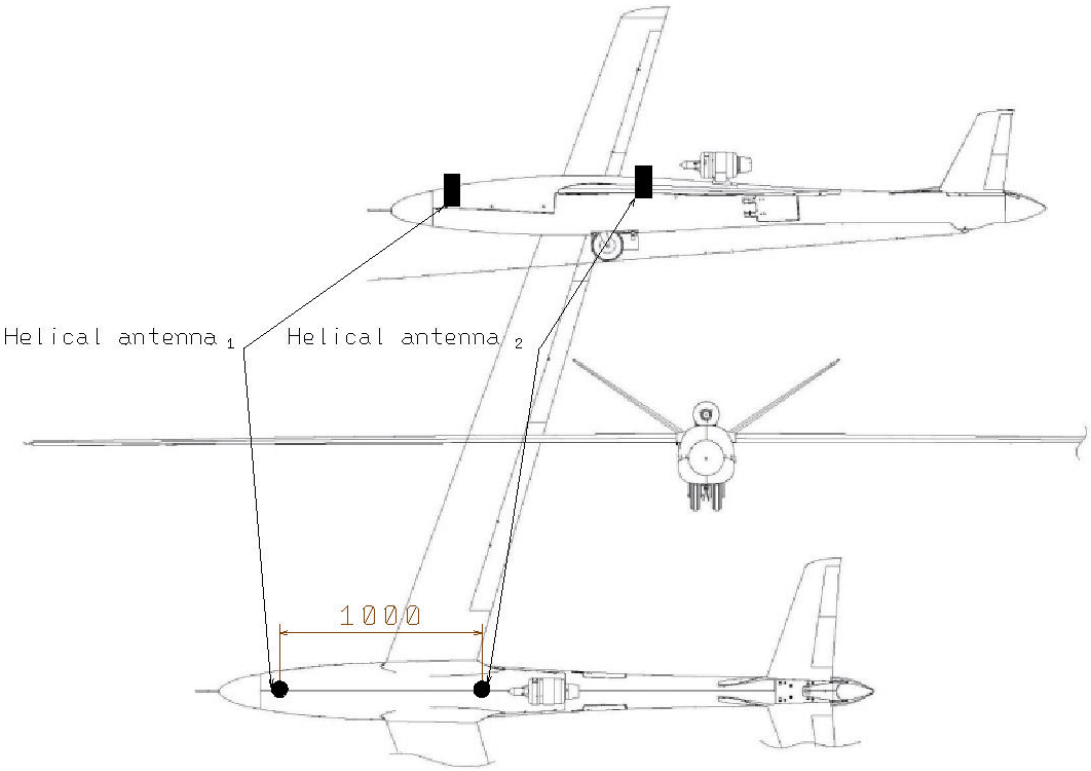

Figure 16: Hardware placement

3 Wing-3

In the previous project FLEXOP, the wing components(airframe, avionics, and controller) were designed almost separately by different expert teams working only in loose cooperation. The control design barely influences the frozen upstreaming aeroelastic design. The interaction between aeroelastic and control was not fully exploited. In order to achieve advanced, actively flight condition optimized wing design, a collaborative design toolchain will be set up through integrating the separately existing tools in each discipline. A new wing (Wing-3) will be derived from this toolchain and serve as a safe and reliable experimental platform to validate the accuracy of the developed toolchain.

The detailed objectives of Wing-3 are to validate that the ASE MDO toolchain is able to provide further benefits via an optimized design leading to the following benefits with respect to the conventional baseline design:

- decrease the flight drag,
- suppress the flutter phenomena better,
- alleviate the gust load and maneuver load better,

compared with the previous design.

In order to achieve the aforementioned goals, a sensor and actuator concept needs to be proposed. More details would be provided in the following sections.

3.1 Sensors

3.1.1 Inertial Measurement Units

The IMUs in wings -0,-1 and -2 were successfully demonstrated to produce accurate acceleration and gyro-rate signals for the purposes of modal analysis. This was confirmed based on a comparison to high quality sensors during the Ground Vibration Test (GVT). Furthermore in-flight data showed accurate results for modal identification and tracking, despite the short measurement duration on a constant flight point.

For the -3 wing, a re-configuration is proposed as shown in Figure!17. These changes include:

- In-plane measurements (+x direction) to identify and track the non-linear in-plane wing mode.
- Use of gyro-rate data (rather than leading edge - trailing edge sensors) to identify and track the wing torsion mode which is critical for flutter monitoring.

The straight arrows in Figure!17 indicate the linear acceleration sensor configuration, while the round arrows indicate the gyro-rate sensors. In combination with the IMUs in the empenage and fuselage, the new setup increases the number of identifiable elastic modes from 5 to 14.

3.1.2 Visual optic shape monitoring

Two cameras Mobius 1080p HD Action Camera are installed in the fuselage, to record the left and right wing motion in flight. The video footage offers the possibility to determine the deflection by means of image processing tools. Thus, the aeroelastic mode shapes of the wing can be analysed. Apart from readings of the IMUs attached on the wings, the before flight developed simulation models can be validated and updated. Furthermore, if the image processing tools can be used to analyse the wing shape online, the system can serve as a safety feature when it comes to unwanted phenomena like flutter.

3.1.3 Inklinometers

Inklinometers are used to measure angles. Installed at several positions along the wings the twist and therefore the aerodynamic shape can be determined. This provides information on the lift distribution, which is useful for a drag control system. It is then possible to optimize the drag by adapting the lift distribution.

3.1.4 Strain gauges for load measurements

In order to identify wing loads, it is proposed to install strain gauges in the -3 wing. Within the framework of the Skopinksi method [7] for strain based load identification, a FE model of the -3 wing will be coupled with a genetic algorithm to optimise the strain

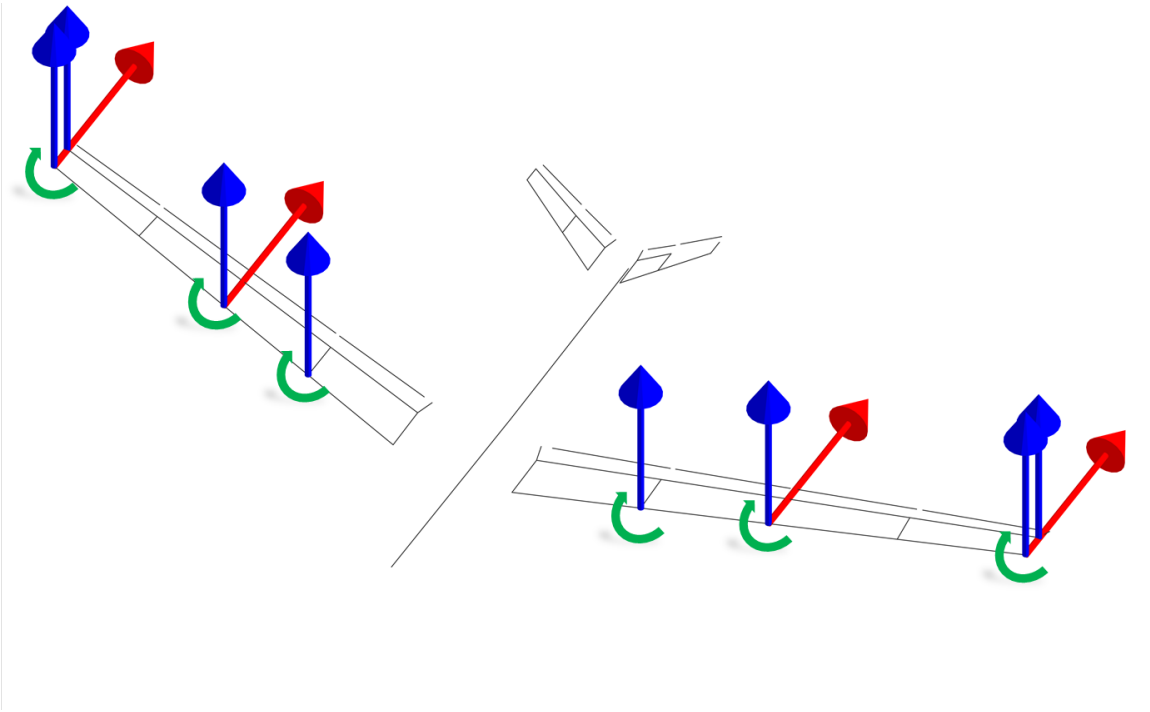

Figure 17: IMU configuration for -3 wing.

gauge locations. The Wheatstone bridge circuits will be measured using instrumentation amplifiers and can be logged on the Flutterometer. The goal of the load data will be comparison with the coupled FE-CFD load predictions. In order to realize strain based load prediction, a Skopinski calibration procedure will be performed during the GVT of the -3 wing set.

3.1.5 Pressure-measuring Wing Glove

To provide additional insight of pressure distribution in-flight, a pressure-measuring wing glove system is in development. The goal of the system is to first provide pressure distribution in a cross-section of a wing in-flight on a UAV with help of Micro-Electro-Mechanical-Sensors (MEMS). As an example, successful project developed by Christian Raab and Kai Rohde-Brandenburger in “In-Flight Testing of MEMS Pressure Sensors for Flight Loads Determination” is taken [6].

Firstly, the wing glove system was adapted for use on UAVs instead of sailplanes. Thus, minimizing size (and especially thickness) is of primary concern during the development. The small scale of the flight-testing platform shall promote data gathering by reducing risk and preparation time per flight test. Secondly, the system shall measure the pressure distribution not only during steady state flight and flow conditions, but also during maneuvers and unsteady flow conditions. This aspect forms an advantage over wind tunnel testing, since a larger variety of conditions can be investigated.

To enable that advantage a sufficient sampling rate is another crucial design requirement. Thirdly, it shall be possible to integrate the system both as a retrofit solution and as a component in newly developed wings. Consequently, modularity and adaptability are another key development objective.

The design solution for the Wing Glove system is subdivided into the electronic system and the hardware fairing. While the fairing development (which will be most relevant for the retrofit version) has not started yet, considerable effort has already been put into the design of the electronic system.

The electronic system will consist of several data aggregators or “slave nodes”, which are controlled by one central master unit. A slave node will consist most notably of eight of the most modern piezoresistive pressure MEMS, a flash buffer memory, and a low power microcontroller mounted to a flexible PCB. It will be thinner than 1.5mm and will measures pressure and temperature at up to roughly 50Hz. The master unit will comprise mainly a microcontroller and a micro SD card port to store the data and it will be of similar thickness as a slave unit. Slave nodes and master unit will be connected via a linear bus and it will be possible to position the slave nodes independently from another and the master unit. In a first prototype the amount of slave nodes will be limited to six. The final system, however, is planned to handle up to 32 slave units or 256 sensors.

3.2 Flight Control system

3.2.1 Control surfaces

When it comes to gust load alleviation, manoeuvre load alleviation, flutter control and drag reduction a high number of control surfaces distributed along the wings is beneficial as this enlarges the controllability. All partners involved in the control activities of the project have the experience with over-actuated systems. However, as the integration of control surfaces is complex and entails an increase in weight due to the actuation system, the number of control surfaces needs to be limited.

With the toolchain developed during this project, a maximum of 16 control surfaces(flaps) can be put to each wing, which results in maximum 32 control surfaces over the overall wing area [2].

3.2.2 Actuator and Monitoring system

That increased surface number will drive the number of actuator significantly high.

Depending on the final flap number of the wing-3, there is three possible solution for the actuators and their monitoring. In the following part of the section the possibilities of these solutions will be discussed.

- PWM based actuators & SHM
- Pure CAN based actuators
- PWM based actuators with ACMU

PWM based actuators & SHM

This solution is similar to what the system already has in all wings. For detailed description see the deliverable 3.1 Report on demonstrator detailed design [4].

The main limitation of this comes from the avionics design itself. Similar problems was driving the development of the custom FCC in the FELXOP project. Driving that many actuator via PWM signals, and still be able to control each of them individually, requires a hardware configuration, which would drive up complexity both in hardware and software.

The current RX-MUX system would allow to increase the number of actuator by 9, by activating the 4-th RX-MUX unit onboard. But above that number, the FCC design does not allow more PWM based actuators. The extra actuator would be freely controllable by the autopilot, but from the pilot side all had to be connected to an already existing control channel.

To have the minimum required monitoring system on board, each actuator has to be fitted with one SHM unit. Although the SHM system proved to be precise and stable enough during operations, assembly and maintenance of the actuators are inconvenient and wearisome. Also it involves permanent damage to the actuator housing.

The main advantage is that any kind of actuator which has sufficient torque/speed ratio can be used for this. The actuators easily can be varied based on the torque/speed requirements of the given surface.

Pure CAN based actuators

Off-the-shelf CAN based actuators can potentially be used. For example Hi-Tech MD950TW-CAN. That have all the required measurements for monitoring already built in. Along with that they also provide current measurement, and the temperature sensor is placed inside the house of the actuator.

Although, the PWM channels are not usable any more in this case, there is no need to add additional SHM units to each actuator. This potentially reduces the system complexity in terms of wiring and assembly.

In terms of performance, there is small variety of actuators, which are available with CAN input instead of PWM input.

Integration with the current FCC system has limitations, although possible. To have maximum use and be able to store all the measurement data, the RX-MUXv2 is needed.

This solution would provide all the necessary data for evaluation of extended or many flap design.

PWM based actuators with ACMU

A third solution for the actuator system would be a custom designed actuator control and monitoring unit(ACMU). The main design features are collected in the following list:

- Monitoring functions:
  - Current
  - Voltage
  - position of actuator level arm
  - position of flap itself

  - temperature
  - run/use time.

- Control function:
  - user-defined control loop and limits
  - discrete state-space controllers
  - actuator detachment on demand — electrically

- Communication:
  - CAN bus

Along with the features listed above, the main design drive is to be able to apply this extra unit to the any PWM driven actuator without physically damaging the servo itself.

This solution would provide all the necessary data for evaluation of extended or many flap design. Also would allow integrate the low level position control loops at the actuator level, and shape the position control performance if necessary.

3.2.3 Standard PWM vs Bus based actuators

This section show a comparison table 1 of the main properties between actuators with monitoring function. One case is, when the monitoring fiction is applied alongside the control inputs in a separate data communication channel. In our case, the control signal are PWM signals, and the monitoring signals from SHM are collected via a CAN bus.

The second case is, when control and monitor function signals are not separated to two physical channels. In a CAN based actuator or in the ACMU, the control monitoring information uses the same CAN-bus for a given set of actuators.

3.2.4 Summary

Based on the previous sections, a purely CAN bus based actuator system should be used in the future. It give requires less mechanical work during assembly and maintenance, also reduces the system complexity, by removing additional cabling and monitoring units. In both cases, a bus based system will provide more feedback data, and open up possibilities for more in-depth analysis and research into actuator systems.

	control and monitoring separated	control and monitoring on the same channel
difficulty of Assembly	depends on the monitoring device, but complicated more cabling	easy, when connectors are used, less cabling
scalability limits	available PWM ports	bus-bandwidth, available channels
operations limits	has to set in FCC or in transmitter	can be set locally
control	PWM	depends on the manufacturer
data feedback	Depends on the monitoring unit, position, temperature	normally position, temperature, current and voltage, usage data
market accessibility	many performance needs accessible	manufacture dependent, normally low range in performance
available bandwidth	high, but depends on the number of the used buses	lower, but depends on the used buses

Table 1: Comparison table between controlling and monitoring designs.

4 Flight control actuator monitoring system experiences

To get information about actuators and theirs position, we use a Servo Health Monitoring System (SHM), which are connected to servos. During flight data analysis, we found that the measured values does not follow accurately the control commands, so we performed an investigation to find it's reason and find a way of a calibration to get higher accuracy position data.

The Source of Data

- The flight logs that were used are from the flight named no. 6 of FLEXOP project
- The control surface calibration data based on a table provided by TUM

Processing of Data

A Matlab script were created to turn raw log data of an actuator into readable charts and repeat the method on every single channel.

Position measurement and temperature data is filtered by the following: High spike (invalid data) detection and elimination (if only a single data is 0.1° or $1^\circ C$ higher/lower than both neighbor data).

On computed difference (and also on the temperature only where compared to that): simple averaging with a 100 sample size window (it is 0.5 s)

Highlighted events during flight

- standing on ground
- braking on ground.
- accelerating on ground.
- take-off and elevating
- switching to flight mode
- flight
- switching to landing mode
- descending
- airbraking

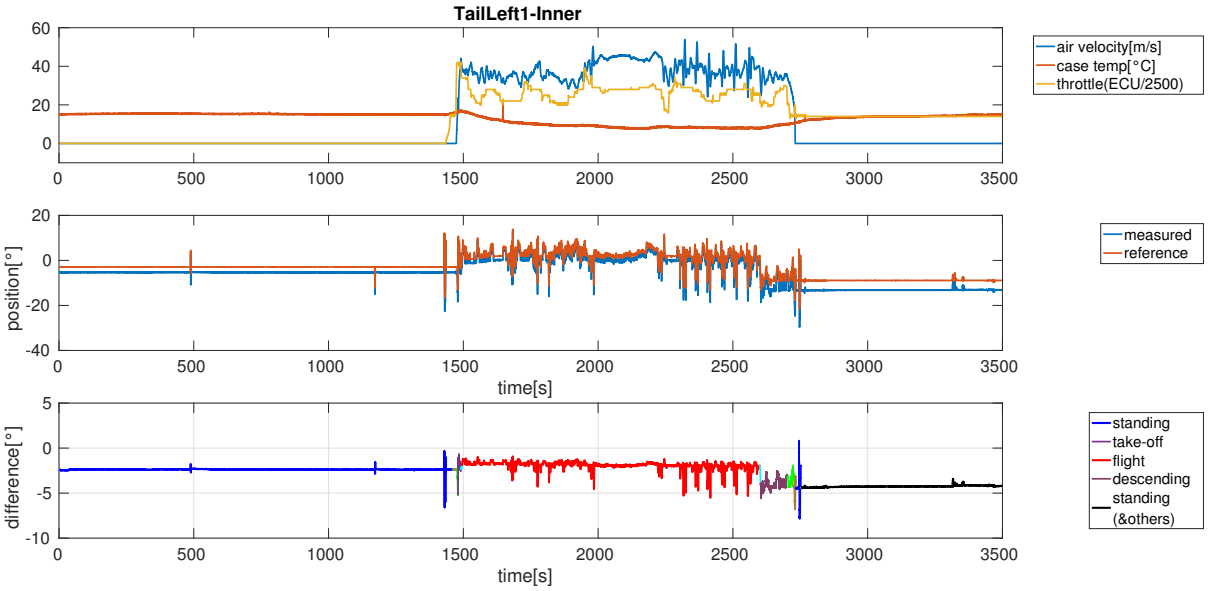

Figure 18: Control surface deflections and servo temperature during whole test

- land
- braking1
- moving on ground
- braking2
- standing on ground and other things after

All these events are calculated from / triggered on the outstanding changes of different data channels. For example jumps in airspeed, or in actuator commands, etc. Figure 18 showing actuator surface deflections in degree, calculated from SHM raw measurement by calibration data.

4.1 Offset in calibration

On many figures (example below) while signals are in a quasi-steady phase, offsets can be observed. Inaccuracy of calibration data can cause offsets and gain errors in data comparison.

Also it is visible on flaps, in different flight states (constant commands with huge difference), the difference of flaps on the right about $1.8°$, and on left $0.7°$ when aircraft switched to landing state. Not the actual deflection differs, but it could be the result of the excel table values may outdated.

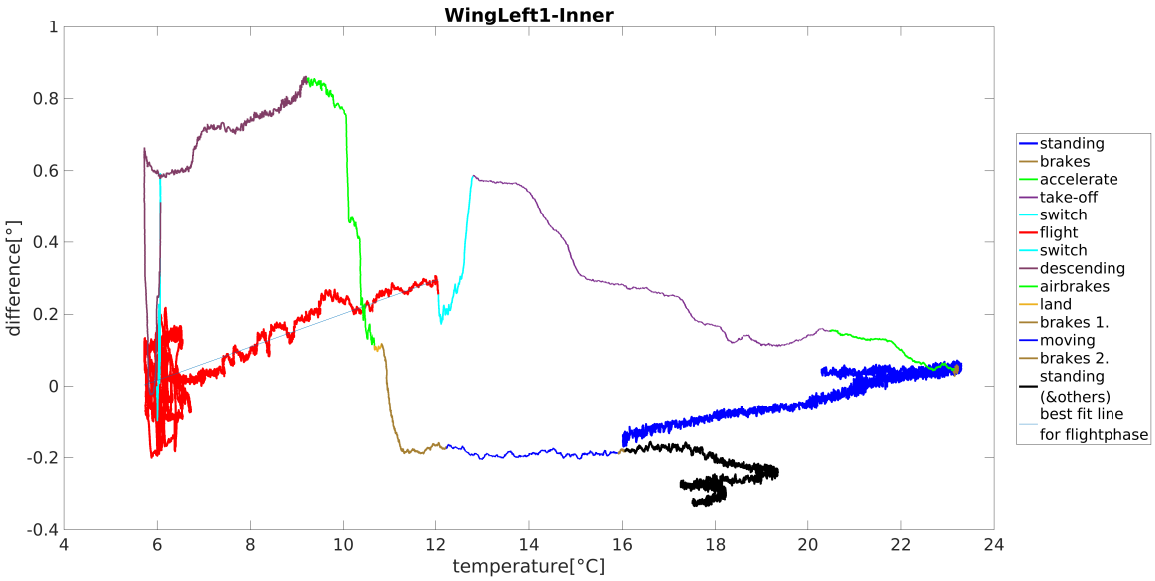

Figure 19: Difference by temperature

On figures, (of flaps) zoomed on take-off period, there is a rising difference over time,

which is due to rising indicated air speed and deflected flaps to generate lift force. It is not a measurement error.

On figures, zoomed on landing sequence, also there is a more bigger position difference, because flaps are moved to high deflection in order to make braking force.

4.2 Creeping of measured position

On full time figures can be noticed, that reference position is constant over 25 minutes, but measured position is climbing slowly, and it produce a varying error. This measurement error is between small boundaries, on land the maximum change is about 0.5 degree, while in air it is 0.2 degree.

The asymmetric mounting of servo bays cause the negative on right and the positive relation between temperature and error on left side actuators. Also any symmetrical correlation in the two sides could not be the result of servo measurement error o, however aerodynamic forces can be both type. And also if we match it to the temperature there is a significant, nearly linear correlation, shifted by the effect of different forces in different states. Colors are showing the elapsing time on the following graph. It is observable, that the start of the take-off is at $15°C$ SHM temperature, and during take-off it cools down to $10.5°C$. During flight, there is a difference under $0.5°C$ and the temperature decreases to around $7°C$ and not changing much. During - from flight

Figure 20: Control surface deflections and servo temperature during take-off

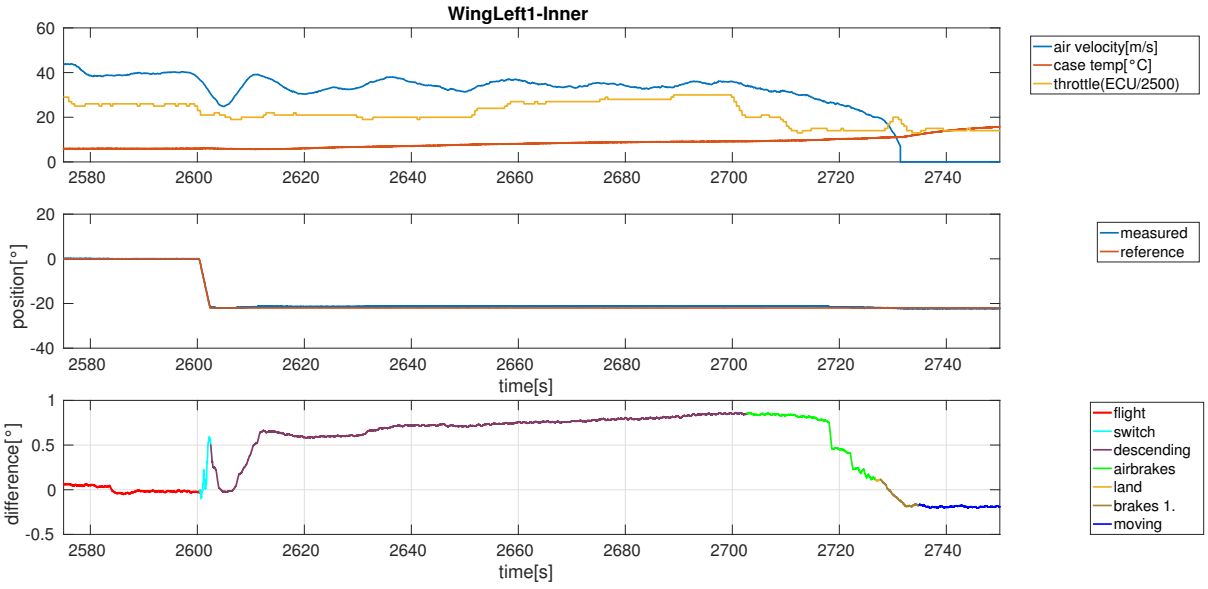

Figure 21: Control surface deflections and servo temperature during landing

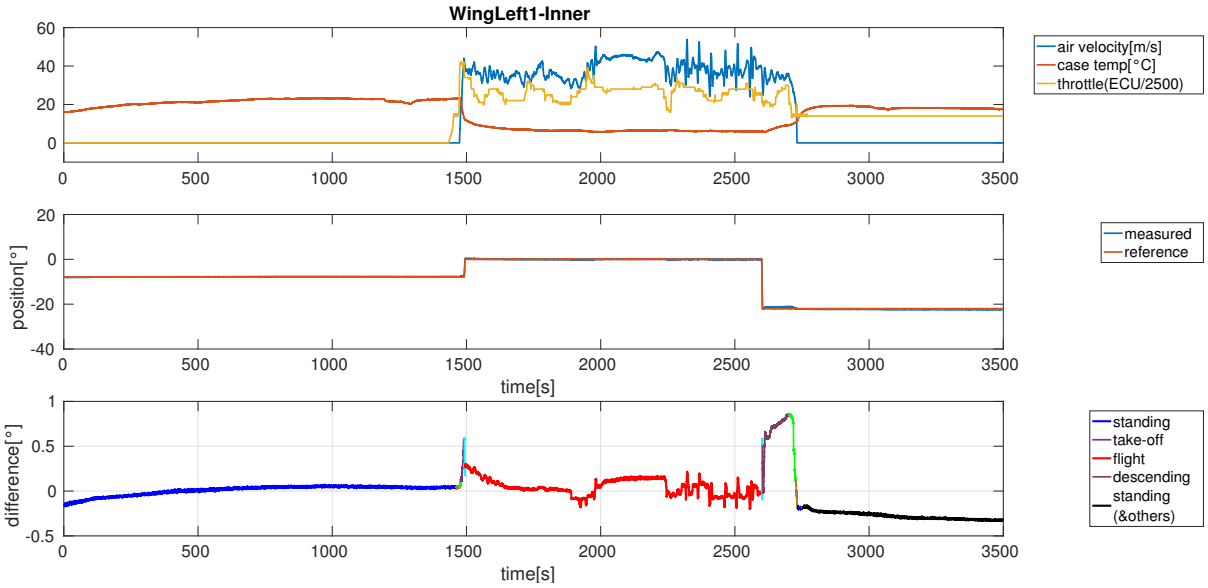

Figure 22: Control surface deflections and servo temperature during the whole test

state switch to descending -, the difference increases to 2° due to aerodynamic forces, (the temperature is still $7^{\circ}C$). During landing, the error slowly changes because of temperature is increasing due to velocity dropping is weakening the cooling effect.

4.3 Test measurement of a servo error in laboratory (SZTAKI)

Compilation:

- prepared a servo(8.4V—max10A) with an SHM unit,
- full FCC stack: Pi, HAT(25.2V—max1.5A), 2*RXMUX(8.4V—max1A)
- Graupner RC
- hot air gun

Separator columns in plot:
Created from RC throttle command pulses, triggered manually during test for timing.

- heating of servo (312-325 s)
- heating of SHM (590-692 s)

Figure 23: Lab measurement system

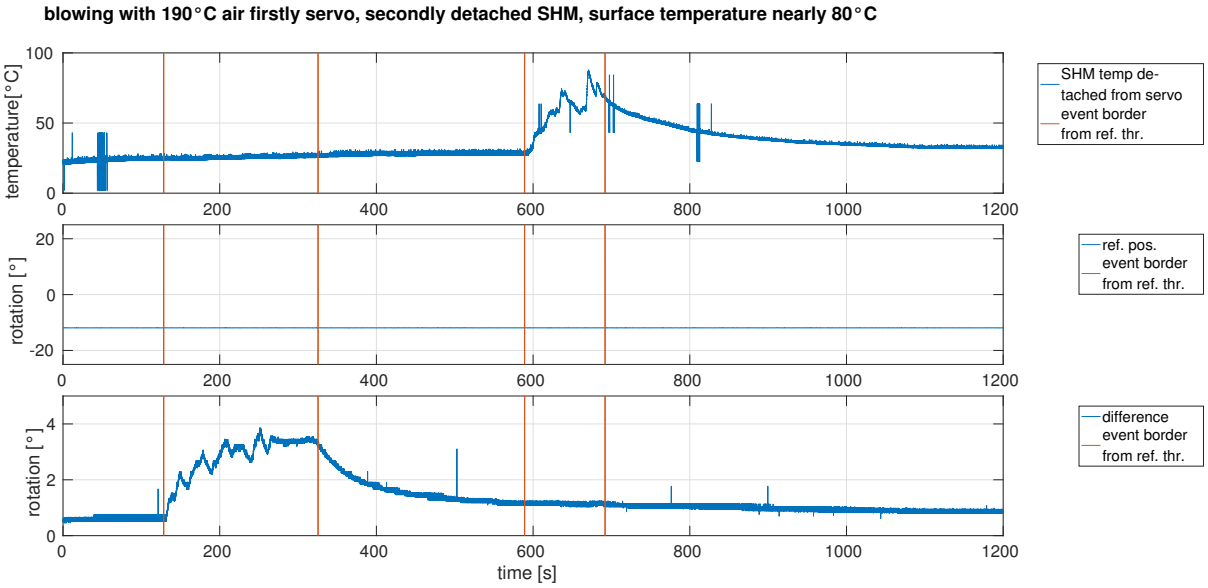

Figure 24: Effect of arbitrary servo heating on SHM measurement difference

- give torque pulses on servo (1230-1340 s)
- heating and torque on servo (1495-1745 s)

4.4 Test results

On figure 24 there is the effect of heating various devices.

Firstly, only the servo is in high temperature, as it seems on plot1/1: no heating on SHM sensor and significant change on position.

Secondly, at 600 sec. It shows the heating of SHM board, SHM sensor temperature is increasing, but no change in position.

That means, separating the heating, separate the error too. So measurement error by temperature is only in the servo itself.

On figure 25 torque was given.

First, only torque,

At 1490s torque and heating servo together.

There is no significant change in the amplitude of error in different position while torque is given, temperature error is similar. Therefore torque is giving an additional error, not proportional.

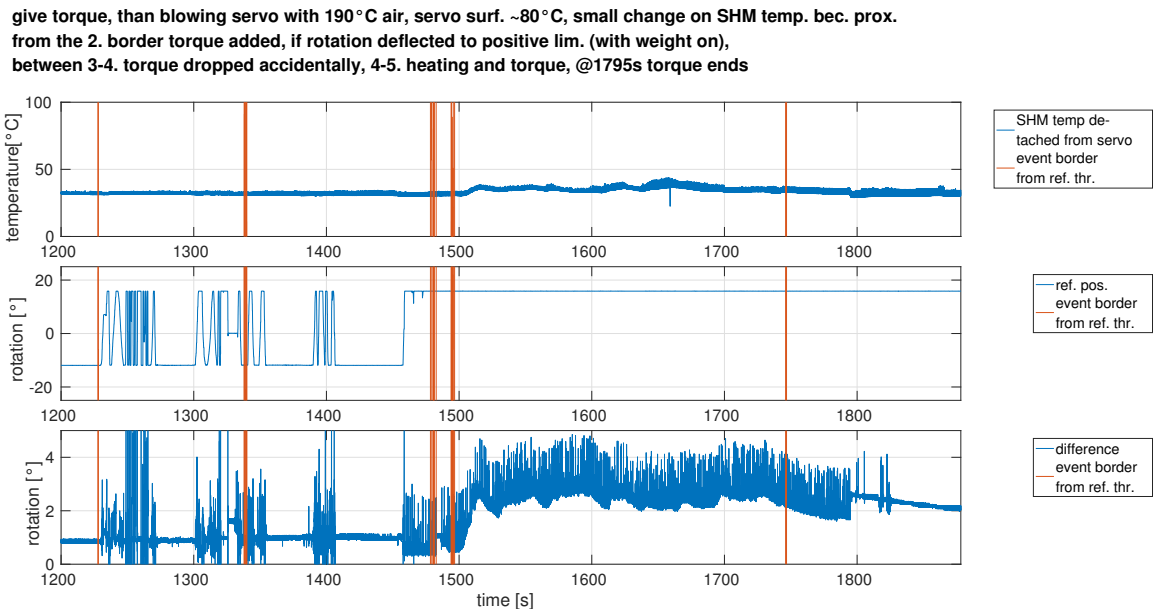

Figure 25: Effect of heating

4.5 Summary

Main sources of position measurement:

- reference trough transfer function of servo and aerodynamic laws
- measurement error due to temperature (almost linear)
  $err_{meas,temp} \simeq coef * (T - T_0)$
- calibration error (sitting on the top of the aboves)

In order to eliminate the two type of error, we assume the nonlinear curve with its piece-wise linear approach, than the error coefficient ($coef_{calib}$) and the additional error ($offset_{calib}$) of calibration are different for every line segment. Position and difference:

$$pos_{measured} \simeq coef_{calib} * (pos + err_{meas,temp}) + offset_{calib}$$

$$diff_{measured} = pos_{measured} - ref \simeq coef_{calib} * pos - ref + coef_{calib} * err_{meas,temp} + offset_{calib}$$

If we did a right calibration of control surfaces (at temperature T_0) and calibration gives a best fit calibration line for segments.

$coef_{calib} = 1, offset_{calib} = 0$, for every segment

There are two option to calculate correlation between measurement and temperature, one is through measured position, or the measured position difference to reference.

	1	2	3
1	'servo'	'a1 [°/°C]'	'a0 [°]'
2	'WingLeft4-Outer'	0.1373	-0.1460
3	'WingLeft3-MidOuter'	-0.1146	1.8455
4	'WingLeft2-MidInner'	0.0181	-0.1780
5	'WingLeft1-Inner'	0.0463	-0.2612
6	'WingRight1-Inner'	-0.0619	0.4513
7	'WingRight2-MidInner'	-0.0675	1.4881
8	'WingRight3-MidOuter'	0.1236	-0.6882
9	'WingRight4-Outer'	-0.0449	0.0658

Figure 26: Best fit line parameters for temperature to measured position

	1	2	3
1	'servo'	'a1 [°/°C]'	'a0 [°]'
2	'WingLeft4-Outer'	0.0472	-0.2616
3	'WingLeft3-MidOuter'	0.0616	-1.0798
4	'WingLeft2-MidInner'	0.0915	-1.8264
5	'WingLeft1-Inner'	0.0462	-0.2603
6	'WingRight1-Inner'	-0.0608	0.4467
7	'WingRight2-MidInner'	-0.0503	1.2417
8	'WingRight3-MidOuter'	-0.0584	1.1005
9	'WingRight4-Outer'	-0.0628	0.2176

Figure 27: Best fit line parameters for temperature to calculated difference

$$pos_{measured} \simeq pos + coef_{temp} * (T - T_0)$$

$$diff_{measured} \simeq diff + coef_{temp} * (T - T_0)$$

Examining both, correlation between measured position (raw data) and temperature is giving different results in different servos, fig.26. But with the calculated difference it can be recognized, fig.27.

The temperature error is not depending on the absolute position, it is an additive error. Thus, subtracting the reference position results in an error with less disturbance from commanding, because position and reference is close to each other due to control loops. We apply the correction to the position difference and not to the raw measurements.

Assuming $diff_{measured} \simeq a_1 * T + a_0$, $a_1 = coef_{temp}, a_0 = diff + coef_{temp} * T_0$

According to measurements $coef = coef_{calib} * coef_{temp} \approx \pm 0.001 \frac{rad}{°C}$ (sign depends on side of AC)

at the end, position datas could be improved:

$pos \simeq pos_{measured} - err_{meas,temp}$

During flight state, temperature cause less then $0.5°$ error in measurement. But calibration error can be a few degrees on some channel.

Notice that, the measured temperature is on the case of the servo not at the potentionmeter, therefor can be a difference between them. So the real temperature is not known, but can be assumed.

Correction of measurement error caused by temperature in servo potentiometer is feasible, since there is a nearly linear correlation between them.

For this, much more precise calibration of control surface is essential, due to calibration error locally could be much higher than measurement error and cannot be distinguish from the effect of temperature.

5 Conclusion

The major outputs of this document are twofold. It proposes changes to the present demonstrator to improve its performance and its data quality. In addition to this, the future system level improvements related to the project goals are also highlighted in the document, what are necessary to demonstrate the validity and benefits of the ASE MDO process. The main outcomes within the documenst are the following:

- Main changes done on the fuselage to operation improvements.
- Additional changes collected for the fuselage, which will further increase operation capabilities.
- Sensoring concept proposed for the wing-3.
- Actuator system concept for wing-3.
- Detailed analysis give on the SHM units thermal sensitivity.

This document will serve for the future as a baseline for detailed wing sensoring and actuator system design.

6 Bibliography

[1] openMCT — open source mission control software. https://nasa.github.io/openmct/. Accessed: 2020-10-22.

[2] Bela Takarics Matthias Wüstenhagen Yasser Meddaikar Fanglin Yu, Thiemo Kier. Deliverable 1.2 - requirements capture for a/c mdo design. *FLIPASED, FLIGHT PHASE ADAPTIVE AERO-SERVO-ELASTIC AIRCRAFT DESIGN METHODS*, 2020.

[3] Edward H. Frank and Jim Lyle. Sbus specification b.o, 1990. http://www.bitsavers.org/pdf/sun/sparc/800-5922-10_SBus_Specification_B.0_Dec90.pdf.

[4] István Gözse Christos Koimtzoglou Franx-Michael Sendner, Philipp Stahl. Deliverable 3.1 - report on demonstrator detailed design. *FLEXOP, FLUTTER FREE FLIGHT ENVELOPE EXPANSION FOR ECONOMICAL PERFORMANCE IMPROVEMENT*, 2019.

[5] s. R. O. JETI model. Ex bus communication protocol, 2013. http://www.bitsavers.org/pdf/sun/sparc/800-5922-10_SBus_Specification_B.0_Dec90.pdf.

[6] Christian Raab and Kai Rohde-Brandenburger. In-flight testing of mems pressure sensors for flight loads determination. In *Scitech 2020 Forum*, January 2020.

[7] Aiken W. S. Jr. Huston W. B. Skopinski, T. H. Calibration of strain-gage installations in aircraft structures for the measurement of flight loads. *NCA Technical Report 1178. Langley Aeronautical Lab. Langley Field*, 1954.